

CHAPTER 4

RESULTS

AND

DISCUSSION

4.1 Characterization of Indolehydrazones and their Metal Complexes

4.1.1 Elemental Analysis

Elemental analysis of the indolehydrazones and their metal complexes shows that the experimental values agree well with the theoretical values. The results are shown in Table 4.1.

4.1.2 IR Spectral Data

The IR data of the ligands and their metal complexes are shown in Table 4.2. The IR spectral data support the evidence of coordination between the metal and the ligand. The $\nu(\text{N-H})$ stretching vibrations of the indole group of the ligands appear in the range 3188-3340 cm^{-1} . These bands are shifted to 3011-3288 cm^{-1} in the metal complexes. This could be due to the presence of the intermolecular hydrogen bonding between the indole hydrogen and the electronegative oxygen atom of the neighboring molecule.

The C=O absorption bands observed in the region 1597-1679 cm^{-1} in the ligands are not observed or shifted upon complexation, suggesting coordination of carbonyl oxygen to the metal ion. Coordination of a azomethine nitrogen to the metal ion is indicated by the shift of the $\nu(\text{C=N})$ of the free ligands at range 1546-1622 cm^{-1} in the metal complexes. The IR spectra of the ligands and their metal complexes are shown in Figure 4.1 – 4.12.

The change in the OH stretching vibration could not be detected, and this might be due to the overlap of the band with N-H stretching vibration. The new bands in the range 426-486 cm^{-1} and 650-677 cm^{-1} were assigned as $\nu(\text{M-N})$ and $\nu(\text{M-O})$ bands respectively.

Table 4.1
Analytical data and some physical properties of indole hydrazones and their metal complexes

Compound	Colour	Melting Point (°C)	Found (Calculated)/(%)		
			C	H	N
2- HapIH	yellow	110-113°C	69.76 (70.59)	4.89 (5.23)	11.85 (13.73)
Zn ₂ - HapIH	white	> 300 °C	61.84 (63.96)	4.31 (4.47)	10.86 (11.85)
Ni ₂ - HapIH	white	> 300 °C	56.99 (61.30)	3.99 (4.56)	9.93 (10.66)
Cu ₂ - HapIH	white	> 300 °C	59.51 (64.13)	3.77 (4.49)	11.04 (11.77)
4-F-2-HapIH	white	105-107°C	66.25 (66.67)	4.54 (4.63)	11.55 (12.96)
Zn ₄ -F-2-HapIH	white	> 300 °C	53.09 (60.73)	3.06 (3.96)	7.93 (11.80)
Ni ₄ -F-2-HapIH	white	> 300 °C	56.99 (61.30)	3.99 (4.00)	9.93 (11.91)
Cu ₄ -F-2-HapIH	white	> 300 °C	49.93 (60.88)	3.50 (3.97)	7.93 (11.83)
5-CH ₃ -2-HapIH	yellow	103-110°C	69.96 (67.86)	5.73 (5.36)	12.11 (12.50)
Zn ₅ -CH ₃ -2-HapIH	white	> 300 °C	62.77 (62.00)	4.83 (4.66)	10.42 (11.42)
Ni ₅ -CH ₃ -2-HapIH	white	> 300 °C	63.36 (62.57)	4.83 (4.70)	10.63 (11.52)
Cu ₅ -CH ₃ -2-HapIH	white	> 300 °C	70.09 (62.16)	5.91 (4.97)	12.21 (11.45)

Table 4.2

IR data for indole hydrazones and their metal complexes (cm⁻¹)

Compounds	$\nu(\text{N-H})$	$\nu(\text{C=O})$	$\nu(\text{C=N})$	$\nu(\text{M-O})$	$\nu(\text{M-N})$
2- HapIH	3188	1672	1622	-	-
Zn ₂ - HapIH	3188	-	1603	665	458
Ni ₂ - HapIH	3048	-	1630	699	474
Cu ₂ - HapIH	3078	-	1546	659	476
4-F-2-HapIH	3254	1679	1660	-	-
Zn ₄ -F-2-HapIH	3011	-	1601	673	459
Ni ₄ -F-2-HapIH	3048	-	1628	673	426
Cu ₄ -F-2-HapIH	3059	-	1612	677	445
5-CH ₃ -2-HapIH	3340	1672	1605	-	-
Zn ₅ -CH ₃ -2-HapIH	3288	-	1618	650	462
Ni ₅ -CH ₃ -2-HapIH	3011	-	1623	585	486
Cu ₅ -CH ₃ -2-HapIH	3193	-	1672	685	421

Figure 4.1
IR spectrum of 2- HapIH

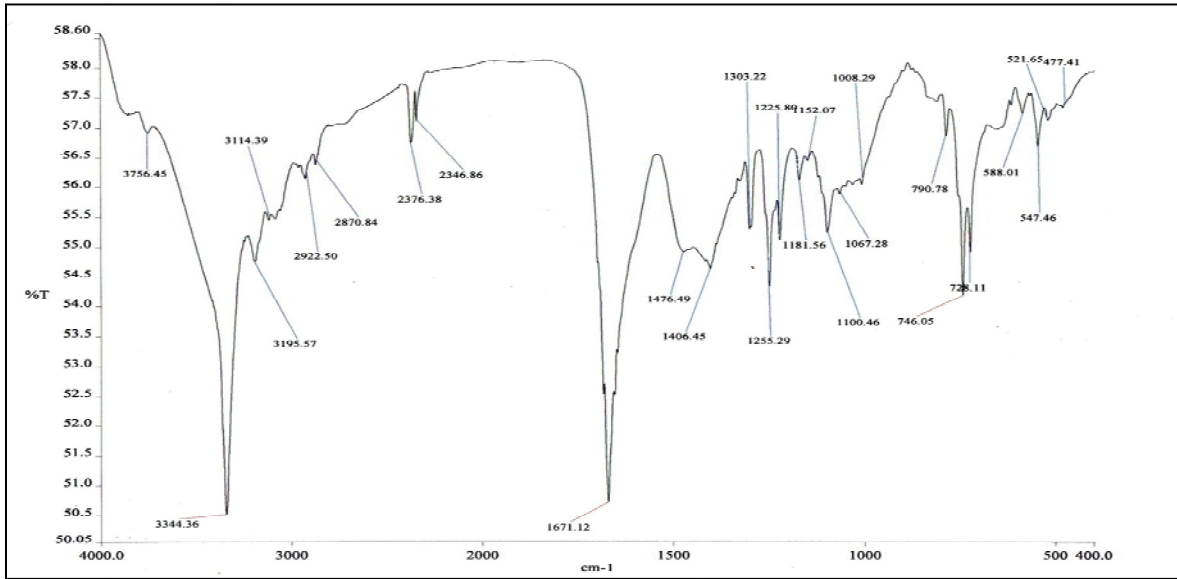
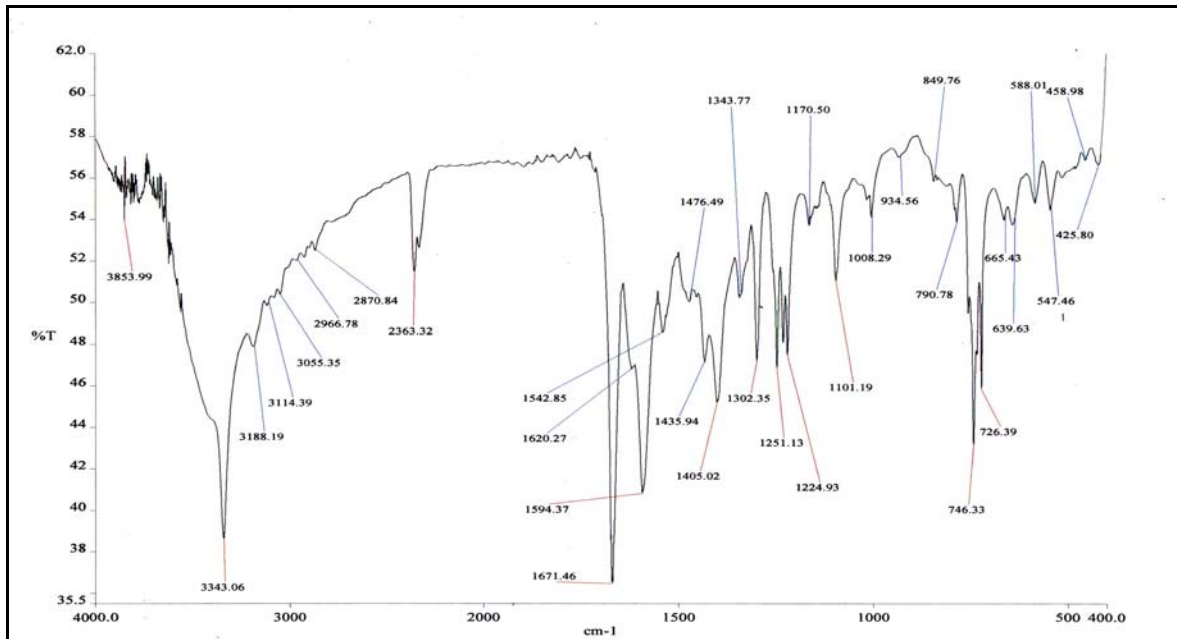


Figure 4.2
IR spectrum of Zn₂- HapIH



4.1.3 NMR Spectral Data

The selected peaks of ^1H and ^{13}C NMR spectra of the ligands are shown in Table 4.3 and Table 4.4. In the spectra of ^1H NMR, the OH and NH signals of the ligands were observed in the region 12.95-13.19 ppm and 11.1-11.85 ppm, respectively. The CH_3 protons of the ligands were observed in 10.85, 10.91 and 10.91 ppm. The aromatic proton of the ligands were observed in the region 6.73-6.89 ppm.

In the spectra of ^{13}C NMR, the C=O and C=N peaks of the ligands were observed at downfield in the region 162.79-168.73 ppm and 131.69-154.82 ppm, respectively. Whereas, the C-OH peaks were observed in the region 136.86-156.29 ppm. The aromatic carbon peaks were observed in the region 167.81-167.99 ppm. The spectra of the ^1H and ^{13}C NMR are shown in Figure 4.12- 4.16.

Table 4.3

¹H NMR data of indole hydrazones (δ , ppm)

Compounds	N-H	O-H	CH ₃	H ₃ aromatic
2- HapIH	11.85	13.19	10.85	6.82-7.59
4-F-2-HapIH	11.12	13.73	10.91	6.89-8.16
5-CH ₃ -2-HapIH	11.10	12.95	10.91	6.73-7.62

Table 4.4

¹³C NMR data of indole hydrazones (δ , ppm)

Compounds	C=O	C=N	C-OH	C aromatic
2- HapIH	168.73	131.69	136.86	167.91-168.73
4-F-2-HapIH	162.79	142.52	143.98	167.81-167.92
5-CH ₃ -2-HapIH	167.82	154.82	156.29	167.99-167.22

Figure 4.12
Schematic ^1H NMR diagram of 2- HapIH in ppm(δ)

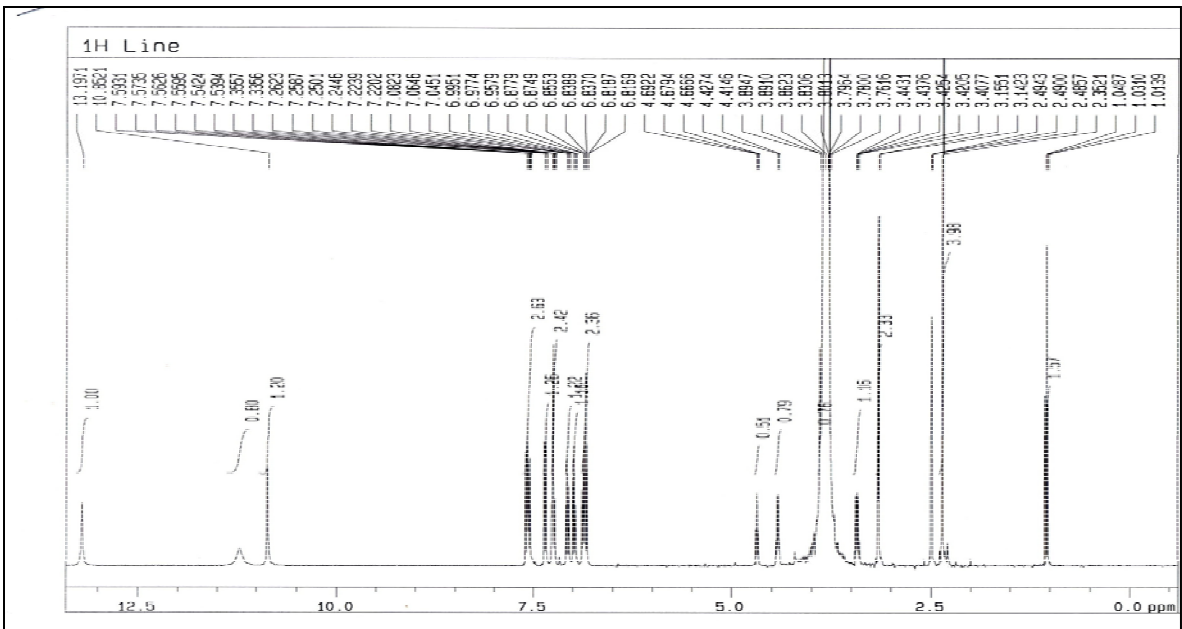
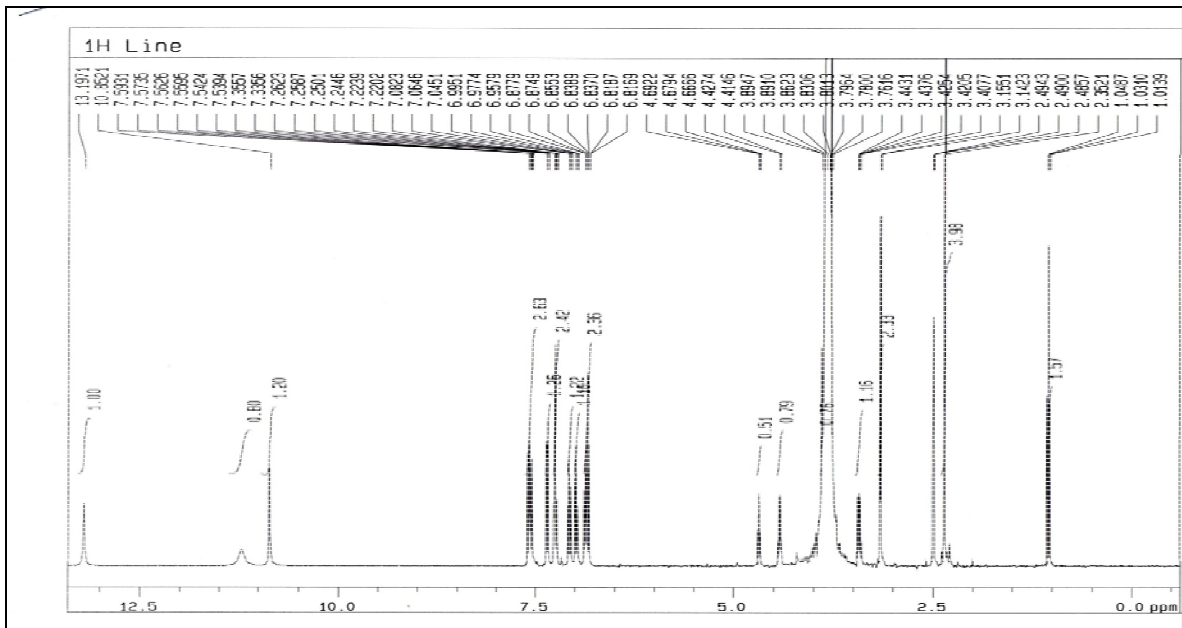


Figure 4.13
Schematic ^{13}C NMR diagram of 2- HapIH in ppm(δ)



4.1.4 UV-Visible Spectra Data

The electronic absorption data of indole hydrazones and their metal complexes, are given in Table 4.5. In the spectra of the ligands, the shoulder bands at 275-298 nm are assigned to $\pi \longrightarrow \pi^*$ transitions associated with indole group and these bands have shifted upon complexation to lower wavelengths in the range 278-280 nm suggesting that the nitrogen atom of the azomethine group is coordinated to the metal ion. This approved that π orbitals covers the hydrazone part of the molecule into the phenyl ring, with the lone pair electrons on the C=O oxygen. While in the spectra of the complexes the less intense and broad bands in the range of 319- 385 nm result from the overlapping of the low energy $n \longrightarrow \pi^*$ transitions mainly localized within the azomethine group at 280 nm. The LMCT (ligand to metal charge transfer bands) transition from the lone pairs of the phenolic oxygen donor to the metal ions were detected in region above 400 nm in the spectra of the metal complexes.

Table 4.5

Assignments of UV-vis spectra data of indole hydrazones and their metal complexes (nm)

Compounds	$\pi \rightarrow \pi^*$ (nm)	$n \rightarrow \pi^*$ (nm)	LMCT
2- HapIH	275	319	-
Zn ₂ - HapIH	291	321	385
Ni ₂ - HapIH	298	385	445
Cu ₂ - HapIH	275	314	371
4-F-2-HapIH	280	355	-
Zn ₄ -F-2-HapIH	295	368	395
Cu ₄ -F-2-HapIH	285	314	368
5-CH ₃ -2-HapIH	280	325	-
Zn ₅ -CH ₃ -2-HapIH	278	335	365
Ni ₅ -CH ₃ -2-HapIH	298	358	415

Figure 4.17
UV visible spectrum of 2- HapIH

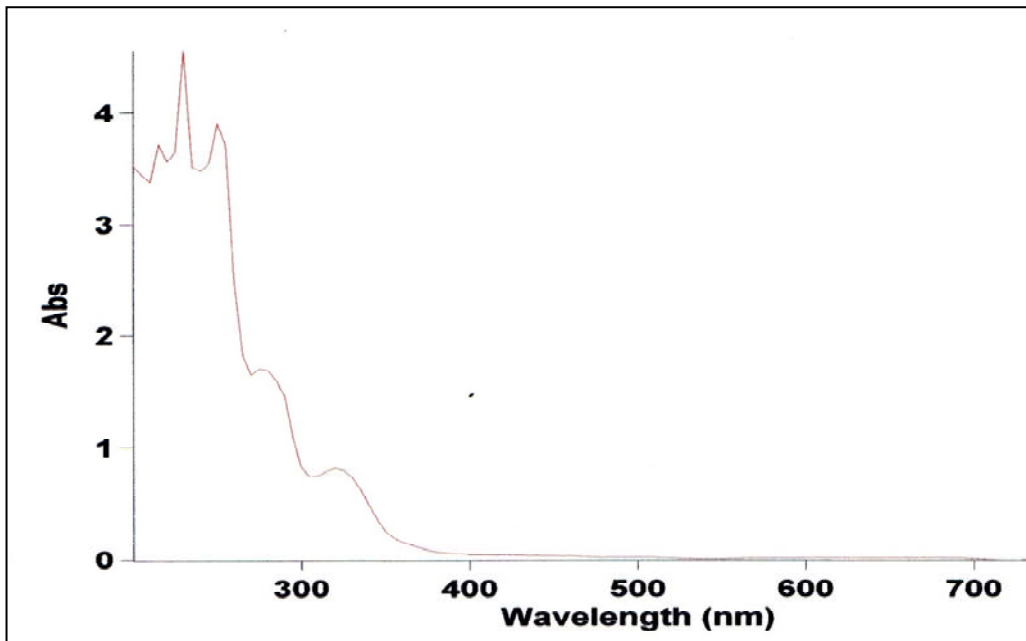
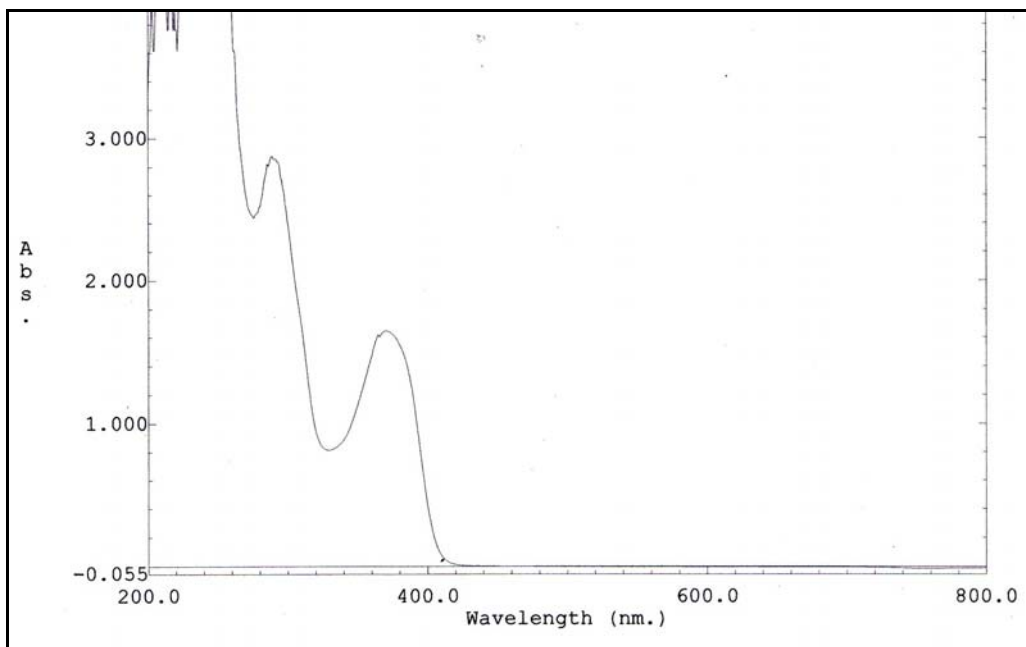
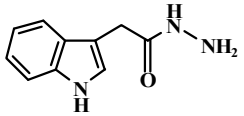
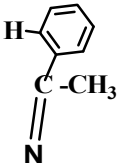
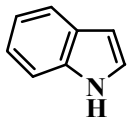
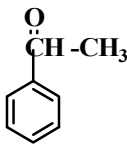


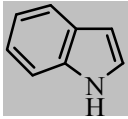
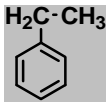
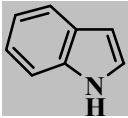
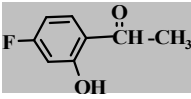
Figure 4.18
UV visible spectrum of Zn₂- HapIH

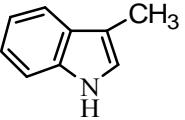
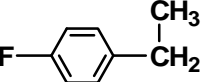
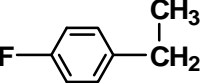
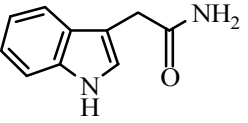


4.1.5 Thermogravimetric Analysis (TGA)

Table 4.6
TGA data of the metal complexes

Compounds	Step	Temperature (°C)	Weight loss (%) Found (Calculated)	Assignment	Residue (%) Found (Calculated)
$Zn_2 \cdot HapIH$	1	35.56-105.5	3.78(2.61)	$2H_2O$	ZnO_2 15.94(13.98)
	2	105.5-350.5	19.90(20.00)		
	3	350.5-710.5	64.16(68.33)		
$Ni_2 \cdot HapIH$	1	30.94-210.5	6.41(5.10)	$2H_2O$	NiO_2 16.06(15.77)
	2	210.5-460.5	48.54(48.70)		
	3	460.5-870.5	23.06(22.3)		
$Cu_2 \cdot HapIH$	1	36.14-1900.5	6.33(5.65)	H_2O	CuO_2

Compounds	Step	Temperature (°C)	Weight loss (%) Found (Calculated)	Assignment	Residue (%) Found (Calculated)
	2	190.5-34.00	27.18(26.10)	H ₂ O	
	3	340.00-460.5	24.83(24.50)		
	4	460.5-620.5	26.09-(27.00)		
Zn ₄ -F-2-HapIH	1	39.8-180.00	13.69(14.5)	H ₂ O	ZnO 59.04(18.60)
	2	180.00-345.00	27.26(27.00)		
	3	345.00-550.00	59.05(59.20)		
Ni ₄ -F-2-HapIH	1	33.8-180.00	45.29(45.50)	2H ₂ O	NiO ₂ 24.38(27.11)

Compounds	Step	Temperature (°C)	Weight loss (%) Found (Calculated)	Assignment	Residue (%) Found (Calculated)
Cu ₄ -F-2-HapIH	2	180.00-410.00	24.39(23.67)		
	3	410.00-540.00	7.67(7.00)		
	1	36.73-100.00	4.52(4.45)	H ₂ O	Cu ₂ O ₂ 16.32(16.12)
	2 3	100.00-198.00 198.00-450.00	2.77(2.81) 44.21(44.81)	H ₂ O	
Zn ₅ -CH ₃ -2-HapIHL	4	450.00-750.00	17.0(12.81)		
	1	33.18-180.5	21.10(20.5)	H ₂ O	Zn ₂ O ₂ 38.74(18.60)
	2	180.5-280.7	7.27(7.30)	H ₂ O	
	3	280.7-390.5	36.05(36.20)		

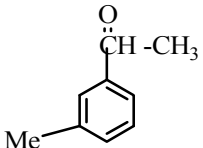
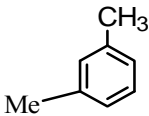
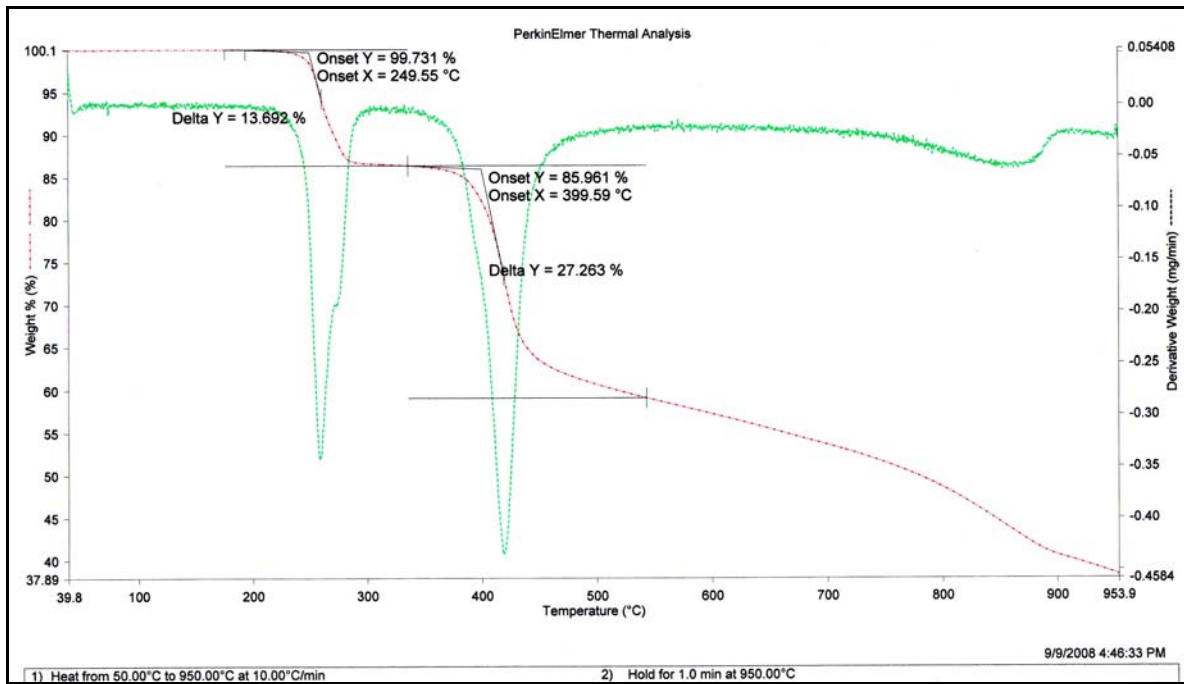
Compounds	Step	Temperature (°C)	Weight loss (%) Found (Calculated)	Assignment	Residue (%) Found (Calculated)
	4	390.5-540.8	17.92(17.6)		
$\text{Cu}_5\text{-CH}_3\text{-2-HapIH}$	1	35.66-138.5	21.59	$2\text{H}_2\text{O}$	CuO_2 41.32(14.24)
	2	138.5-495.00	58.56(57.5)		

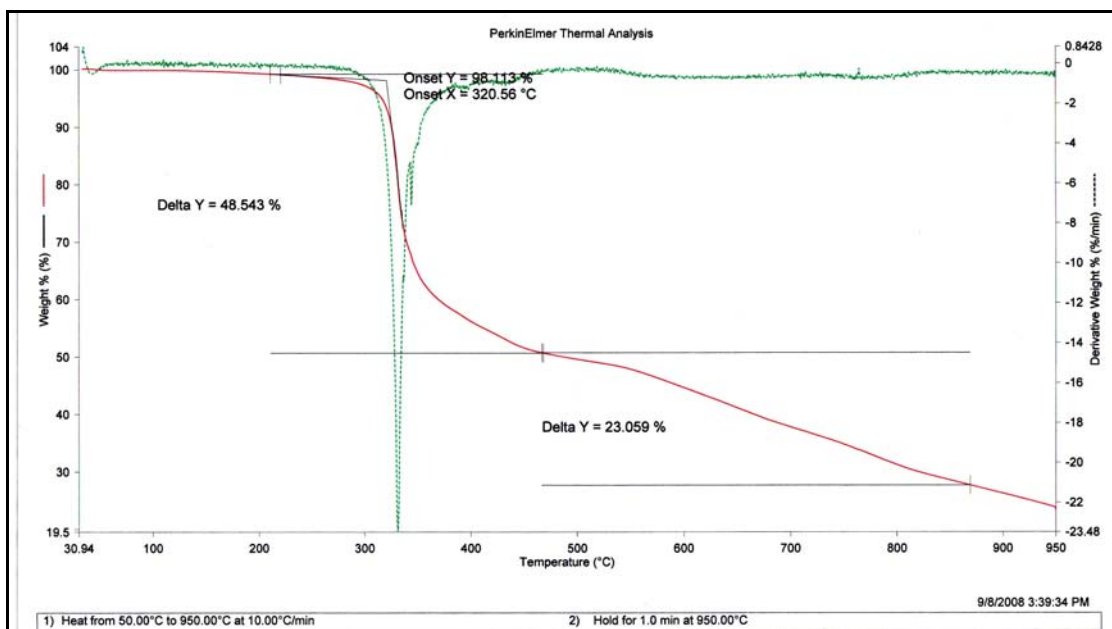
Figure 4.27

TGA spectrum of Zn_2 -HapIH



The Zn_2 -HapIH complex was stable up to 35.56 °C and its decomposition started at this temperature and was completed at 710.5 °C. A mass loss has occurred within the temperature range 35.56 – 105.50 °C corresponding to the loss of hydrated water molecule. The Zn(II) complex decomposed and produced ZnO residue in three steps in the temperature range 35.56-105.5, 105.5-305.5, and 350.5-710.50 °C.

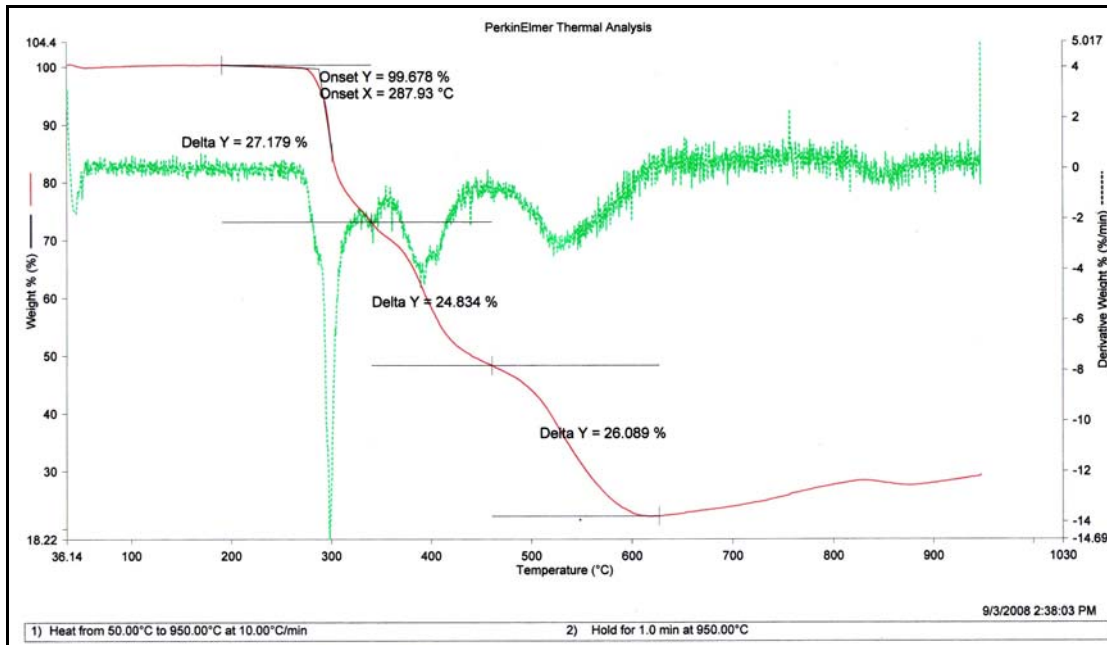
Figure 4.28
TGA spectrum of Ni₂-HapIH



The Ni₂-HapIH complex was stable up to 30 °C and its decomposition started at this temperature and was completed at 870.50 °C. A mass loss occurred within the temperature range 30.94-210.5 °C corresponding to the loss of one hydrated water molecules. The Ni(II) complex decomposed and produced NiO₂ as residue in three steps in the temperature range 30.94-210.5, 210.5-460.50, and 460.50-870.50 °C.

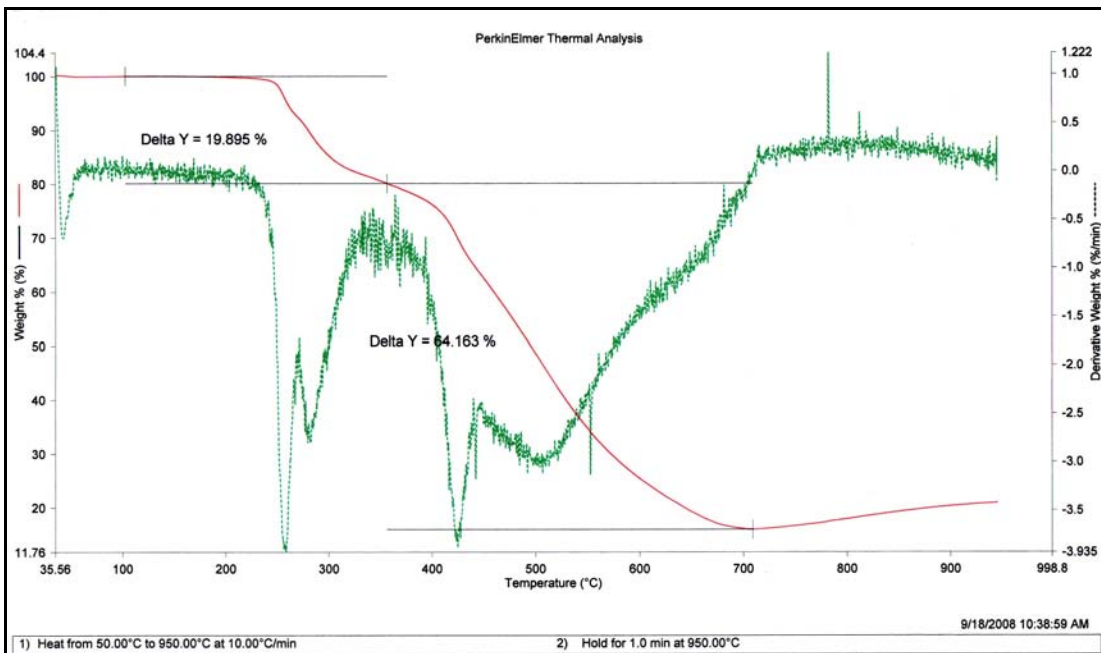
Figure 4.29

TGA spectrum of $\text{Cu}_2\text{-HapIH}$



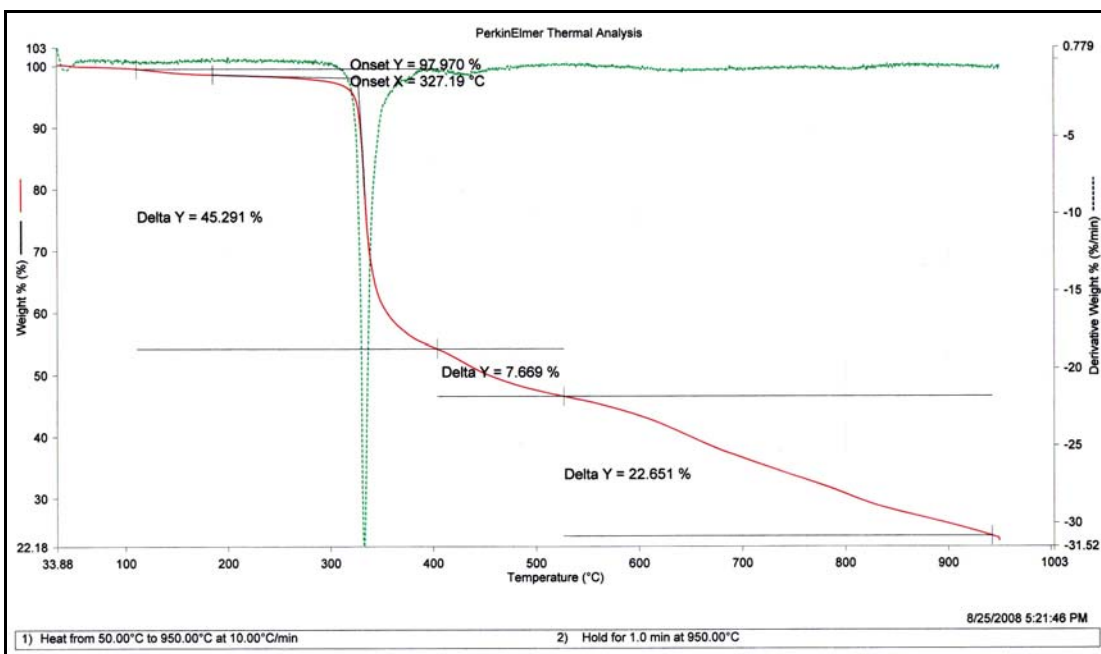
The $\text{Cu}_2\text{-HapIH}$ complex was stable up to 36.14 °C and its decomposition started at this temperature and was completed at 620.5 °C. A mass loss occurred within the temperature range 36.14-190.50 °C corresponding to the loss of two hydrated water molecules. The Cu(II) complex decomposed and produced CuO_2 as residu in four steps in the temperature range 36.14-190.50, 190.50-340.00, 340.00-460.50 and 460.50-620.50 °C.

Figure 4.30
The TGA spectrum of Zn(4-F-2-HapIH)



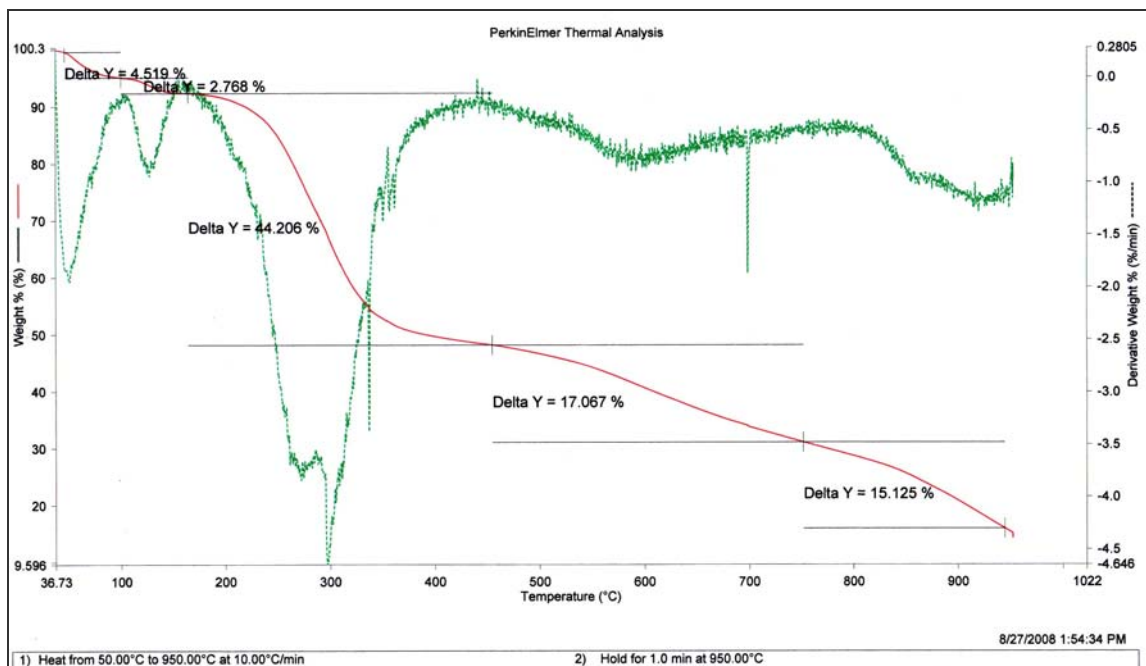
For Zn(4-F-2-HapIH) complex, a mass loss occurred within the temperature range of 39.8-180.00 °C corresponding to the loss of hydrated water molecules and at the temperature range of 180.00-345.00 °C corresponding to a loss of indole moiety. At the temperature range of 345.00-550.00 °C a mass loss occurred corresponding to a loss of 4-fluoro-2-hydroxyacetophenone. The decomposition continues till a constant weight was obtained where ZnO residue was formed.

Figure 4.31
TGA spectrum of Ni(4-F-2-HapIH)



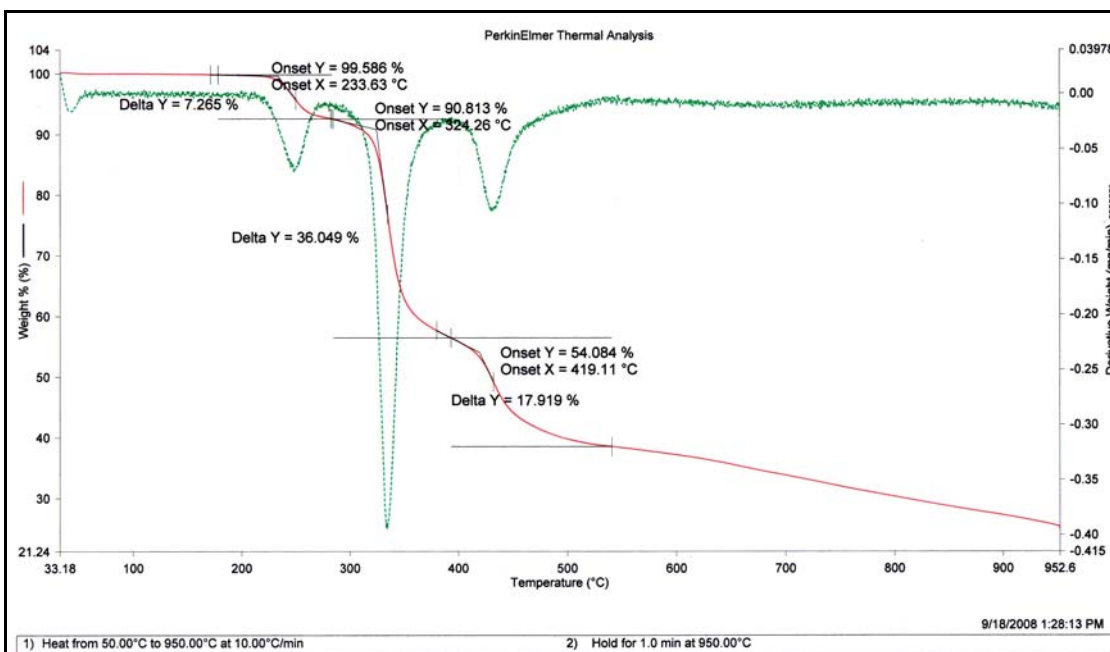
For Ni(4-F-2-HapIH) complex a mass loss occurred within the temperature range of 333.8-180.00 °C corresponding to the loss of two hydrated water molecules and at the temperature range of 180.00-410.00°C corresponding to a loss of indole moiety. At the temperature range of 410.00-540.00 °C a mass loss occurred corresponding to a loss of 4-fluoro-2-hydroxyacetophenone. The decomposition continues till a constant weight was obtained where NiO₂ residue was obtained.

Figure 4.32
The TGA spectrum of Cu(4-F-2-HapIH)



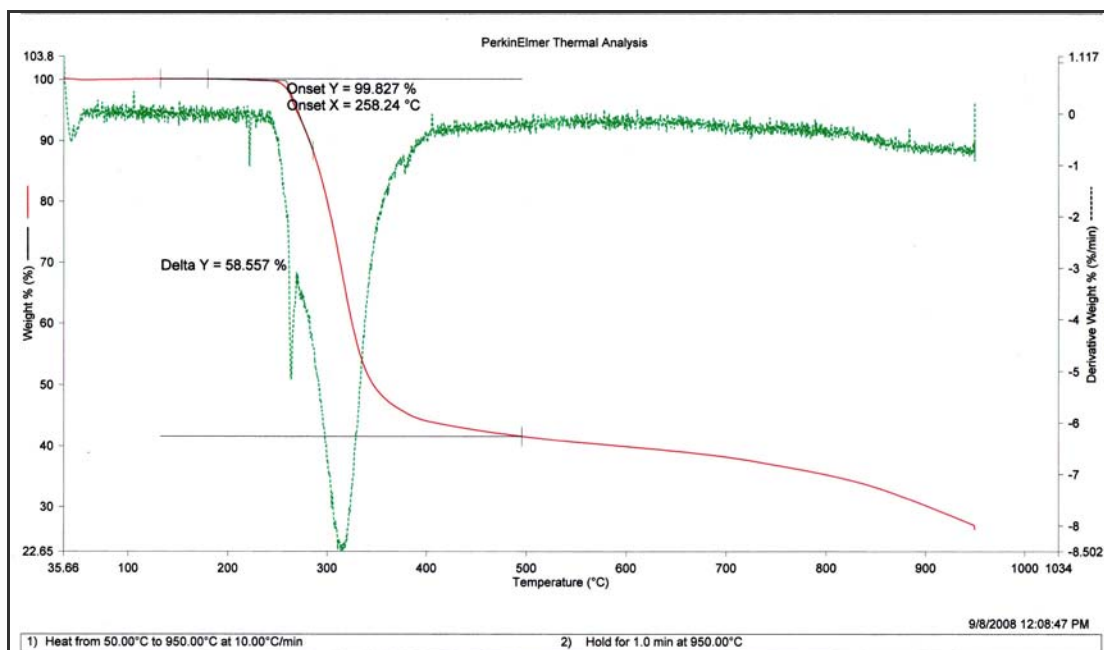
The Cu(4-F-2-HapIH) complex was stable up to 36.73 °C and its decomposition started from this temperature onward and was completed at 950.00 °C. At the temperature range 100.00-198.00°C a mass loss occurred corresponding to a loss of water. At the temperature range of 198.00-450.00 °C mass losses occurred due to the loss of indole group. Finally the temperature range 750.00-950.00 °C mass loss occurred corresponding to 4-fluoro-2-hydroxyacetophenone and this continues till a constant weight is obtained where a copper oxide residue is formed.

Figure 4.33
The TGA spectrum of Zn(5-CH₃-2-HapIH)



The Zn(5-CH₃-2-HapIH) complex was stable up to 33.18 °C and its decomposition started at this temperature and was completed at 540.80 °C. A mass loss occurred within the temperature range 33.18-180.50 °C corresponding to the loss of two hydrated water molecules. The Zn(II) complex decomposed and produced ZnO as residue in four steps in the temperature range 33.18-180.50, 180.50-280.70, 280.70-390.50 and 390.50-540.80 °C.

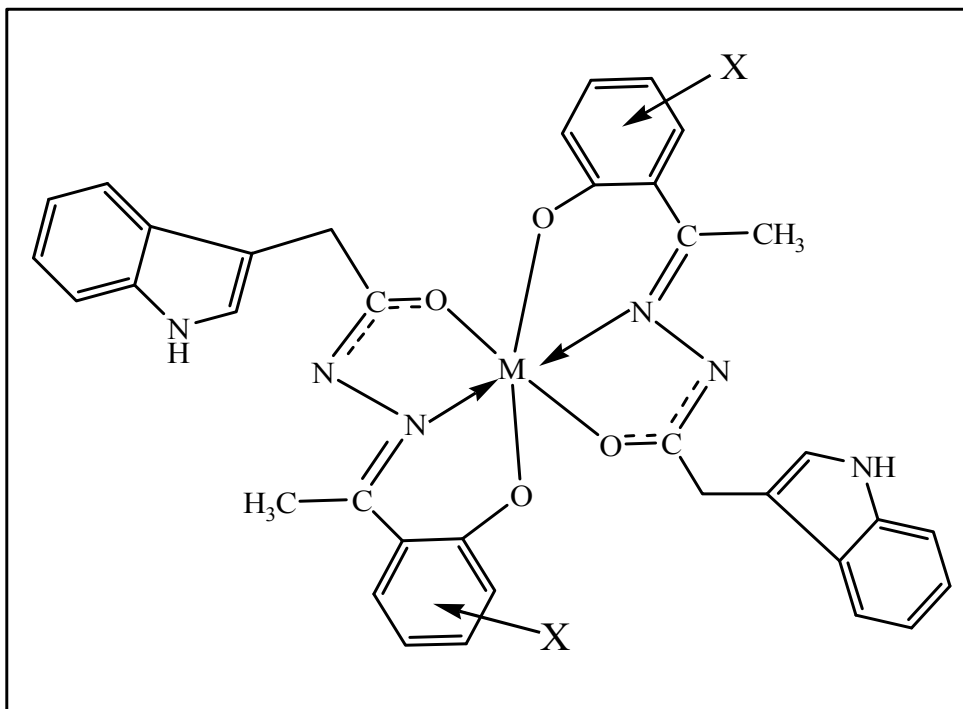
Figure 4.34
The TGA spectrum of Cu(5-CH₃-2-HapIH)



The Cu(5-CH₃-2-HapIH) complex was stable up to 35.66 °C and its decomposition started at this temperature and was completed at 499.50 °C. A mass loss occurred within the temperature range 35.66-138.50 °C corresponding to the loss of two hydrated water molecules. The Cu(II) complex decomposed and produced CuO₂ as residue in two steps in the temperature range 35.66-138.5 °C. and 138.50-495.00 °C.

4.1.6 Conclusions

The proposed structure of the metal complexes is as below :



X = H, 4-Fluoro and 5-CH₃

M = Zinc, Nickel or Copper

4.1.7 Crystal Data

The crystal data of 5-CH₃-2-HapIH is given in Table 4.7. Thermal ellipsoid diagram of 5-CH₃-2-HapIH is depicted in Figure 4.35. A crystal was obtained for the Zn(II) complex of the same ligand. The crystal data is given in Table 4.7 and the thermal ellipsoid diagram of the Zn(II) complex is depicted in Figure 4.36. The dinuclear compound lies about a center-of-inversion. The deprotonated monoanion *O,N,O* chelates to the Zn atom; the hydroxyl oxygen atom also engages in bonding to the symmetry-related Zn atom so that one nitrogen and oxygen atoms comprise a square around the metal. The geometry is a square pyramid, with the apical site occupied by a water molecule. Hydrogen bonds, with the water molecule serving as donor atom, leads to the formation of linear chain motif.

Figure 4.35
ORTEP diagram for the structure of 5-CH₃-2-HapIH

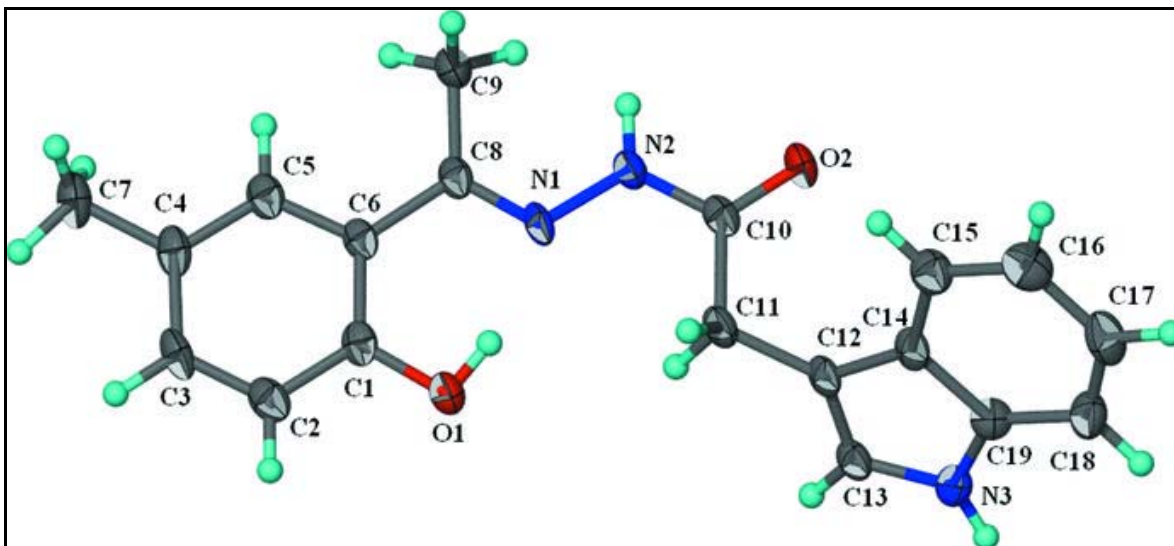


Figure 4.36
ORTEP diagram of $Zn_5\text{-CH}_3\text{-2-HapIH}$

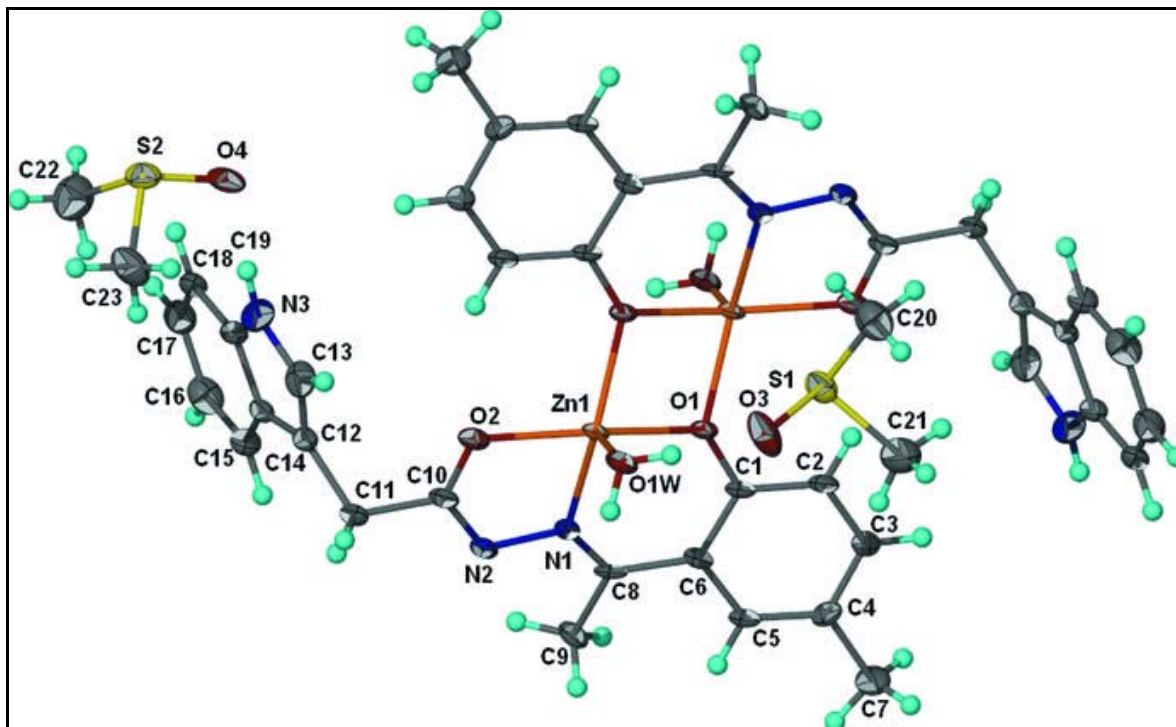


Table 4.7

Crystals data and structure refinements for ligand 5-CH₃-2-HapIH and complex Zn₅-CH₃-2-HapIH

	5-CH₃-2-HapIH	Zn₅-CH₃-2-HapIH
Empirical formula	C ₁₉ H ₁₉ N ₃ O ₂	[Zn ₂ (C ₁₉ H ₁₇ N ₃ O ₂) ₂ (H ₂ O) ₂]
Formula weight	321.37	1118.00
Colour	Yellow	Yellow
Crystal system, space group	Triclinic, PI	Triclinic, PI
Unit cell dimensions	a = 4.6812 (9) Å b = 12.419 (3) Å c = 14.202 (3) Å α = 109.919 (3)° β = 91.710 (3)° γ = 90.751 (3)°	a = 8.5271 (2) Å b = 8.8849 (3) Å c = 16.8279 (5) Å α = 85.519 (2)° β = 84.920 (2)° γ = 84.251 (2)°
V (Å ³)	775.7 (3)	1260.44 (6)
Z	2	1
T(K)	100 (2)	100 (2)
ρ calcd, (Mg m ⁻³)	1.376	1.473
Absorption coefficient (mm ⁻¹)	0.09	1.18
F (000)	340	584
Crystal size (mm)	0.40x0.13x0.005 mm	0.19x0.03x0.03 mm
θ _{max}	3.0-28.3°	2.4-21.0°
Limiting Indices	-6 ≤ h ≤ 3	-11 ≤ h ≤ 11
Limiting Indices	-15 ≤ k ≤ 16	-11 ≤ k ≤ 9
Limiting Indices	17 ≤ l ≤ 18	-21 ≤ l ≤ 21
Reflections collected / unique	3490/4854	13526/5739
R _{int}	0.051	0.077
Data/ parameters	3490/3/231	5739/3/13
Final R indices [I > 2 (I)]	0.060	0.056

4.2 Electrochemical studies of ligands and complexes

The cyclic voltammetry for reduction and oxidation of the ligands and complexes are shown in the Figure (4.37-4.44) and the Table 4.8 and 4.9 gives the selective electrochemical data. The cathodic and anodic peaks were scanned at 10 mV until 400mV scan rate. The difference between the cathodic and anodic peaks (ΔE_p) is indicating that there is one electron transfer in the oxidation of the complexes.. The ratio I_{ap} / I_{cp} shows that the oxidation and reduction of complex is quasi-reversible behaviour. When the potential scan rate ranged from 10 mV/s to 400 mV/s, both anodic peak potential, E_p and peak current, I_p are affected by scan rate as shown in Figure 4.37 and Figure 4.38. As the scan rate increase, the currents increase and the potential shifted to more positive potential. According to Nicholson for an irreversible anodic reaction, the relationship between E_p and v is

$$E_p = E^{\circ} + (RT/\alpha n_a F) [0.780 + \ln (D_R^{1/2} / k^{\circ}) + \ln (\alpha n_a F v / RT)^{1/2}] \quad (\text{Eq 1})$$

By plotting E_p versus $\ln v$ Figure 4.41 and Figure 4.42, the plot show a linear graph for 2-HapIH and in complex $Zn_{2\text{-HapIH}}$. This behaviour obeys the Nicholson's equation and confirmed that the electrochemical oxidation of complex $Zn_{2\text{-HapIH}}$ in this experimental condition is totally irreversible. According to the slope of the straight line of E_p against $\ln v$ the product of αn_a can be evaluated. Plot E_p versus $\ln v$ Figure 4.39 show the slope is 0.0013 while Figure 4.40 show the slope is 0.0011. After simplified the equation, the slope is $RT/2\alpha n_a F$. Therefore, the value of αn_a is 0.99 in 2-HapIH and 1.17 in complex $Zn_{2\text{-HapIH}}$.

Figure 4.37

Cyclic voltammetry of 2-HapIH 10mg with 0.1g TBATFB in 25 ml DMSO, at 10-400 mVs⁻¹, at 25°C.

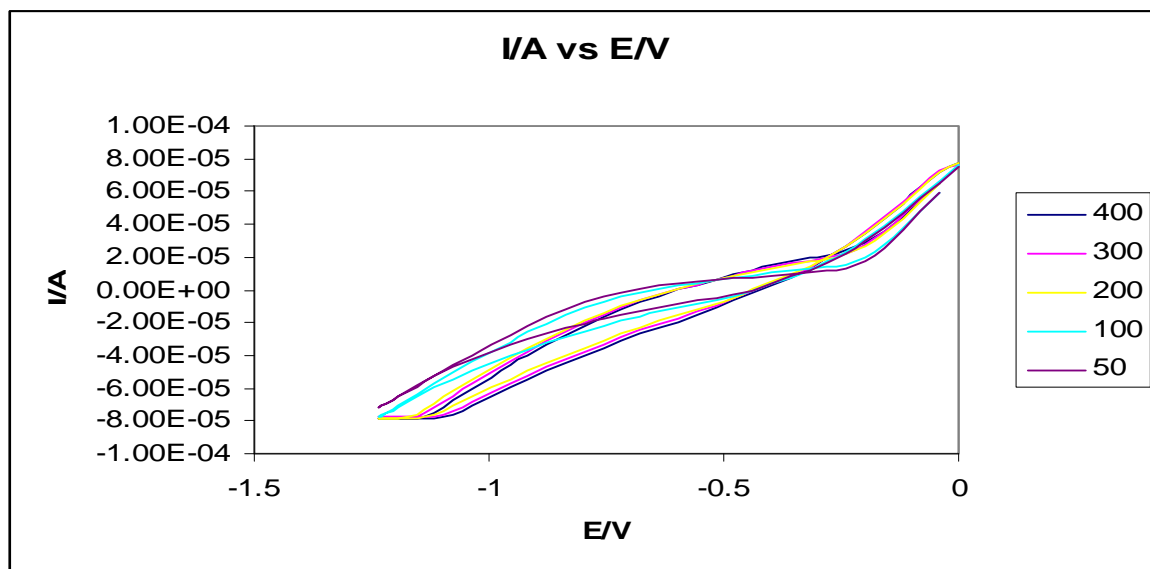


Figure 4.38

Cyclic voltammetry of complex Zn₂-HapIH 10mg with 0.1g TBATFB in 25 ml DMSO, at 10-400 mVs⁻¹, at 25°C.

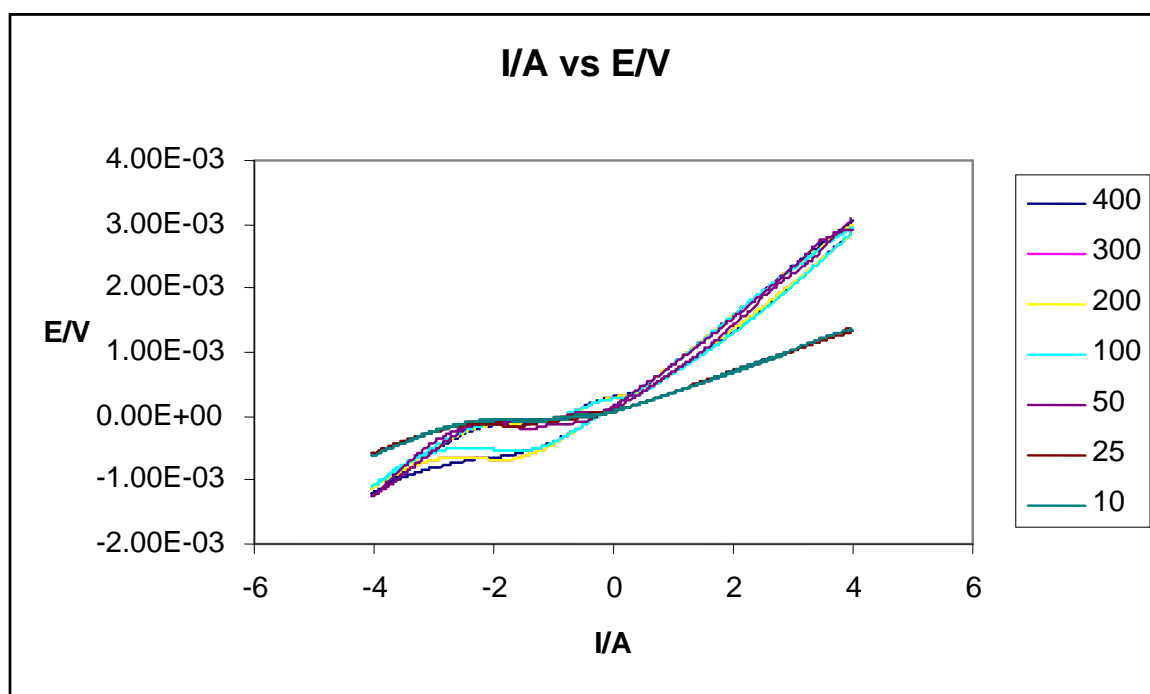


Figure 4.39
The plot of E_p versus $\ln(v)$ of 2- HapIH at 25°

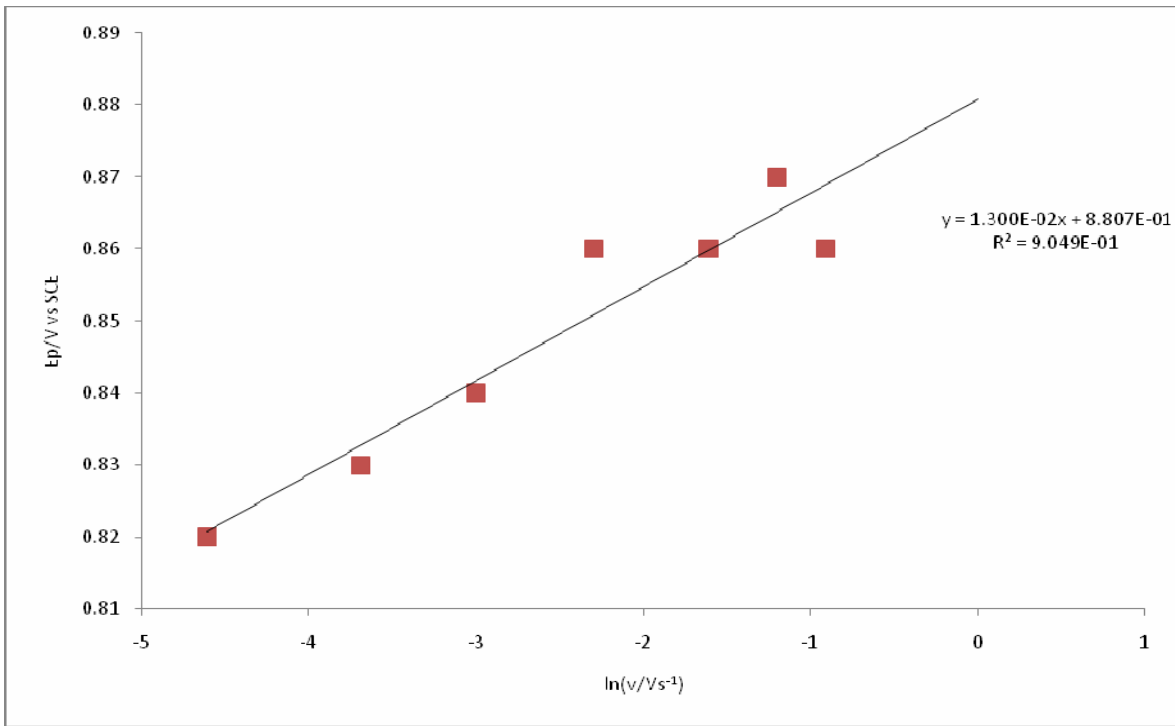


Figure 4.40
The plot of E_p versus $\ln(v)$ of Zn₂-HapIH at 25°C

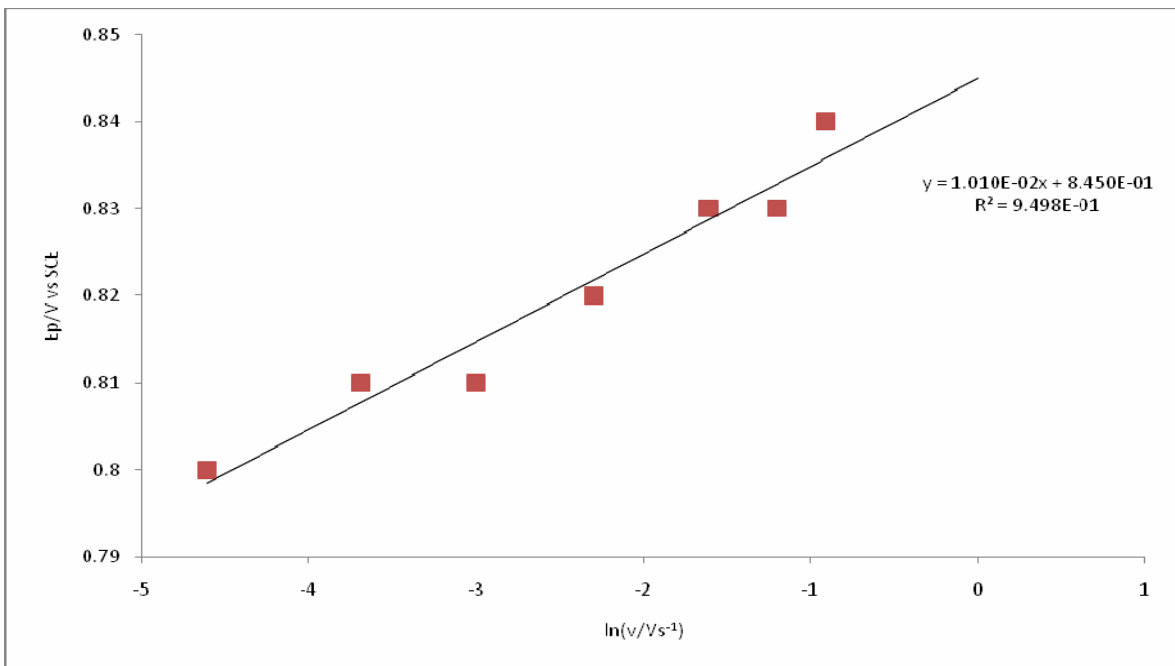


Table 4.8

Cyclic voltammogram data for the oxidation of (a) 2-HapIH and (b) complex Zn_2 -HapIH

V/s	$\ln(v/Vs^{-1})$	(a) $I_p/A (x10^{-4})$	(a) E_p/V	(b) $I_p/A(x10^{-4})$	(b) E_p/V
0.400	-0.90	1.64	0.88	1.36	0.85
0.300	-1.20	1.33	0.86	1.12	0.84
0.200	-1.62	1.13	0.85	1.00	0.83
0.100	-2.31	1.12	0.84	0.75	0.82
0.500	-3.00	0.64	0.83	0.56	0.81
0.025	-3.69	0.52	0.82	0.44	0.81
0.010	-4.61	0.38	0.81	0.30	0.80

In addition, the peak current I_p for an irreversible electrochemical reaction can be described by the following formula

$$I_p = (2.99 \times 10^5) n(\alpha n_a)^{1/2} A C D^{1/2} \nu^{1/2} \quad (\text{Eq 2})$$

According to Eq 2, at a given concentration of 2-HapIH and complex $Zn_{2\text{-HapIH}}$, the plot of peak current, I_p versus square root of the scan, $\nu^{1/2}$ should be linear. From the slope of the straight line, the value of $[n(\alpha n_a)^{1/2} A C D^{1/2}]$ can be evaluated in Figure 4.41 (a) and Figure 4.42 (b) show linear plots of I_p versus $\nu^{1/2}$ was obtained and the parameter of $[n(\alpha n_a)^{1/2} D^{1/2}]$ was calculated as $9.03 \times 10^{-5} \text{ cm s}^{-1}$ for 2-HapIH and $6.99 \times 10^{-5} \text{ cm s}^{-1}$ complex $Zn_{2\text{-HapIH}}$.

Figure 4.41
Plot of I_p versus $v^{1/2}$ for 2- HapIH

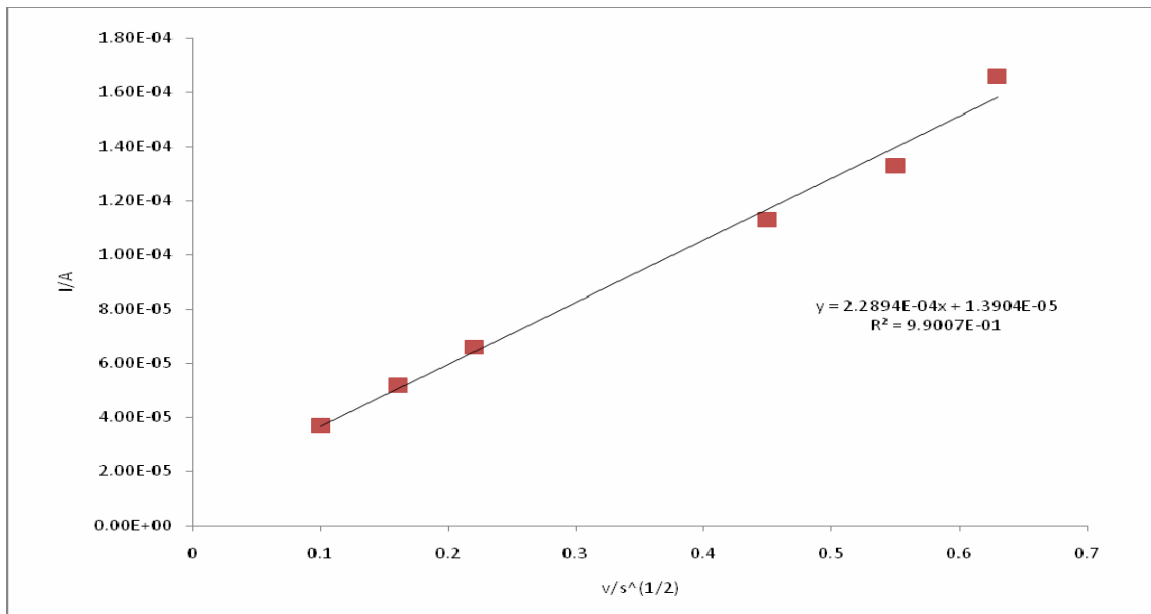
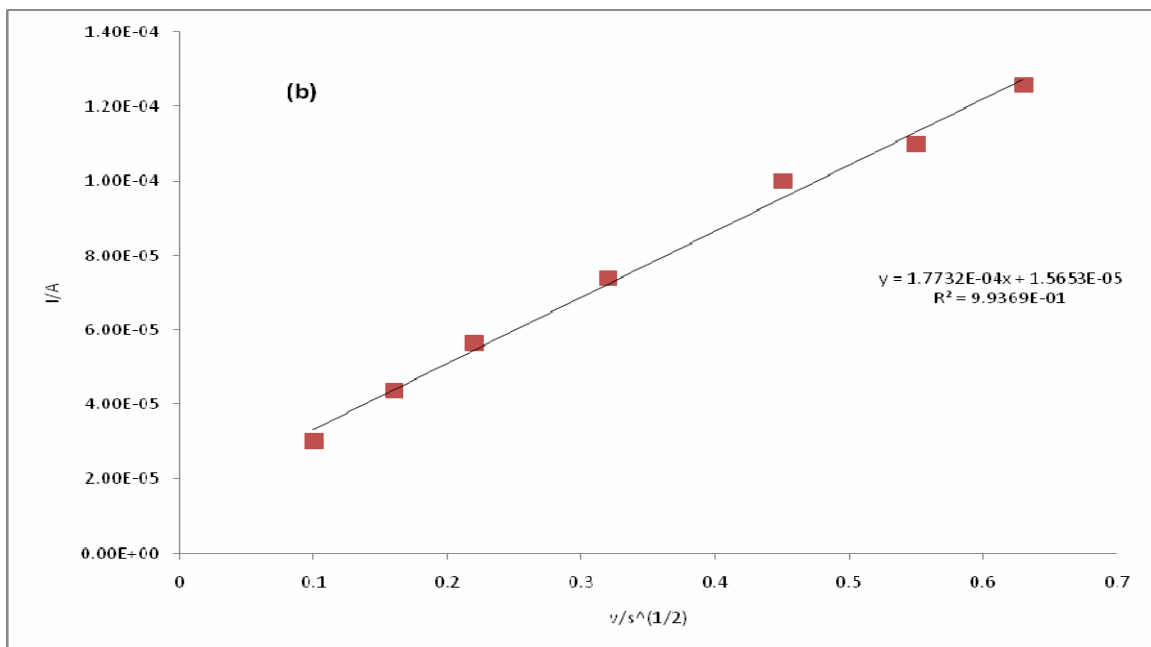


Figure 4.42
Plot of I_p versus $v^{1/2}$ for Zn₂- HapIH



To get the value of n and D , a steady voltammetry of 0.120 M of 2-HapIH and complex $Zn_2\text{-HapIH}$ on the same electrode was determined and shown in Figure 4.43 and Figure 4.44. The limitation diffusion current, I_1 is 8.38×10^{-11} A and 5.80×10^{-11} A respectively. Therefore the value of nD can be calculated as $1.20 \times 10^{-8} \text{ cm}^2 \text{ s}^{-1}$ in 2-HapIH and $8.35 \times 10^{-9} \text{ cm}^2 \text{ s}^{-1}$ in complex $Zn_2\text{-HapIH}$ by using the following formula;

$$I_1 = 4nFDc r \quad (\text{Eq 3})$$

Combining with the value of $nD^{1/2}$ as described previously, the value of D can be calculated as $1.15 \times 10^{-8} \text{ cm}^2 \text{ s}^{-1}$ and $1.67 \times 10^{-8} \text{ cm}^2 \text{ s}^{-1}$ and the value of n can be calculated as 0.83 and 0.71 respectively. Taking account the error of calculation, it was assuming that the number of electron transfer for 2-HapIH is 1. Table 4.9 summarised the data that was evaluated and calculated above. Assuming $n_a = n$, therefore the value of α is 0.99 in 2-HapIH and 1.17 complex $Zn_2\text{-HapIH}$.

Figure 4.43
The steady state voltammogram of 2- HapIH

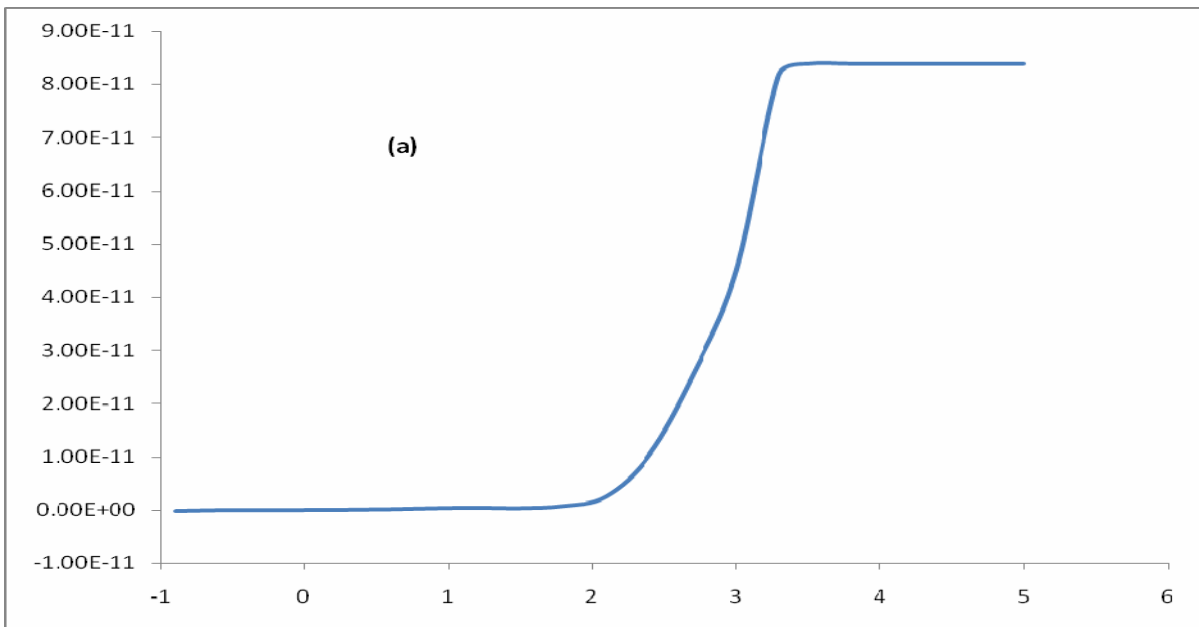
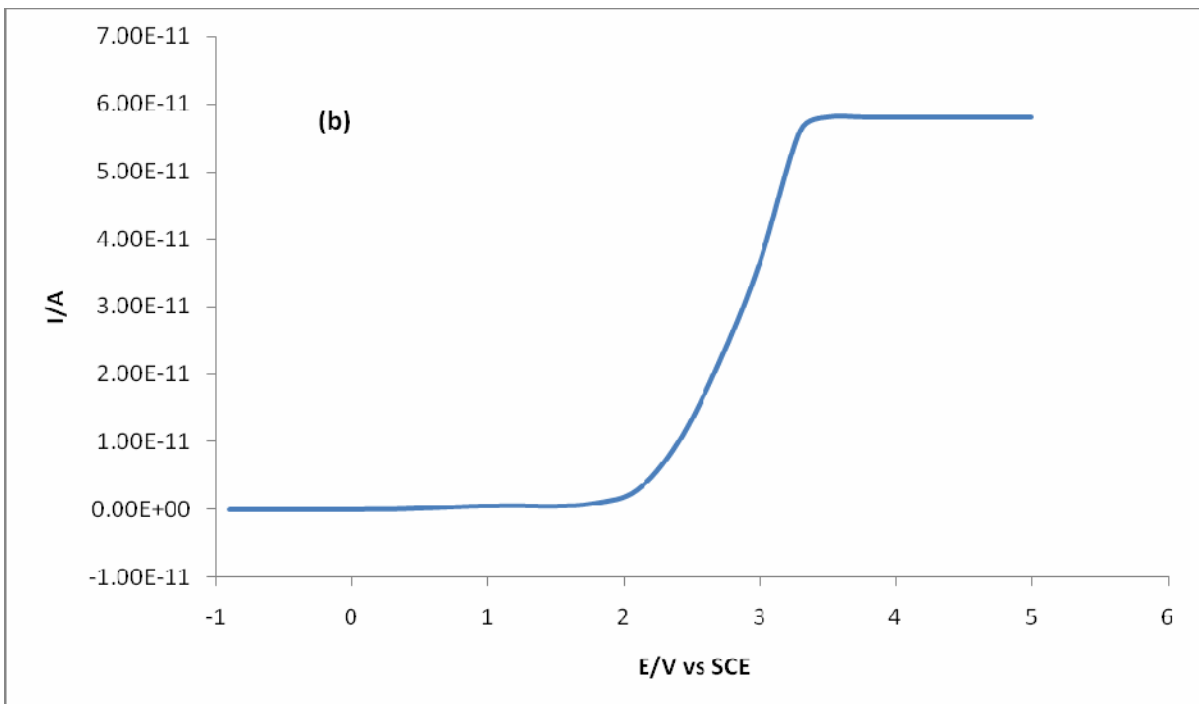


Figure 4.44
The steady state voltammogram of Zn_2 - HapIH



4.3 Anti-ulcerogenic Activity

Table 4.10 shows the anti-ulcerogenic activity of the Schiff bases and their metal complexes. Although the exact mechanism of these drugs is not completely understood, there have been many developments in understanding the factors that control metal binding to possible biological target such as indole derivative complexes. Further studies are required to explore their actual mechanism of action.

Generally all the ligands and their metal complexes except for 2- HapIH and Ni₅. CH₃-2-HapIH show better anti-ulcerogenic activity compared to cimetidine, the standard drug with percentage of inhibition almost over 90 percent. The results also show that substituted ligands inhibit gastric lesion more than the unsubstituted ligand and electron withdrawing substituent shows better inhibition compared to electron donating substituent. This is because the actual mechanisms still not very clear because the scope of my research is limited on screening the inhibition of ulcer. In conclusion, metal complexes show better inhibition of gastric ulcer compared to their free ligands.

Table 4.10

Gastroprotective effect of the Schiff base ligands and their metal complexes and cimetidine on ethanol induced gastric ulcer in rats.

Pretreatment	Mucus Weight (mg)	pH	Ulcerative Lesion Index (Mean \pm S.E.M) (mm ²)	Inhibition (%)
Control (Negative)	3.50	4.43	1510.26 \pm 468.28	-
Cimetidine (Positive Control)	3.63	6.63	170.40 \pm 25.17	89.50
2- HapIH	1.66	5.32	295.71 \pm 35.62	80.42
Zn ₂ - HapIH	1.84	5.12	0.00 \pm 0.00	100.00
Ni ₂ - HapIH	1.88	5.28	100.58 \pm 24.17	93.34
Cu ₂ - HapIH	1.92	5.35	0.00 \pm 0.00	100.00
4-F-2-HapIH	1.78	4.67	33.53 \pm 15.27	97.78
Zn ₄ -F-2-HapIH	1.83	4.98	0.00 \pm 0.00	100.00
Ni ₄ -F-2-HapIH	1.98	4.53	10.73 \pm 5.11	99.29
Cu ₄ -F-2-HapIH	1.25	5.65	22.65 \pm 18.65	98.50
5-CH ₃ -2-HapIH	1.48	4.76	131.69 \pm 27.65	91.28
Zn ₅ -CH ₃ -2-HapIH	1.59	4.35	8.61 \pm 4.58	99.43
Ni ₅ -CH ₃ -2-HapIH	1.77	5.88	312.47 \pm 45.58	79.31
Cu ₅ -CH ₃ -2-HapIH	1.96	5.16	3.78 \pm 8.65	99.75

Data are reported as mean \pm S.E.M